Control of heat transfer in single-story mechanically ventilated double skin facades

Aleksandar Jankovic, Francesco Goia

Department of Architecture and Technology, Norwegian University of Science and Technology, NTNU, Trondheim, Norway

ARTICLE INFO	ABSTRACT
	This paper systematically investigates and quantifies the interplay between mechanical ventilation rate and operation of venetian blinds in determining the performance of a single-story double skin façade. The investigation covers both the supply-air mode and the outdoor air curtain mode of a mechanically ventilated double skin façade. For this experimental study, a full-scale mock-up of a single-story double skin façade was installed in a climate simulator facility and exposed to a series of steady-state regime conditions under two representative cases of temperature gradient and solar irradiance replicating the summer, and the mid-season/winter case. The study results showed the relative weights of the different variables in leading the behavior of the façade. They provided evidence that the control of the performance of a double skin façade may change with the seasons, and that airflow rates and venetian blinds can play different roles depending on the boundary conditions and target performance. Venetian blinds were far more dominant than the mechanical ventilation rate in controlling the net heat transfer in the tested summer conditions, while the opposite was seen for the dynamic insulation efficiency. In mid-season/winter conditions, while operating the façade in a supply-air operation mode, the mechanical ventilation rate was the dominant variable in controlling the net heat transfer. Recommendations for the operation of the double skin façade were also developed as a result of this study. Low and moderate ventilation rates (up to 100 m³h⁻¹ per linear meter of façade) were found suitable to deliver enough fresh air with good preheating efficiency while provide adequate control over the net heat transfer. Higher airflow rates, even in summer peak conditions, were not found to be particularly effective in reducing the solar gain through a façade operated in an outdoor air curtain mode when the interior skin was realized with an insulated glazed unit.

1. Introduction

1.1. Background

Double skin facades (DSFs) are well-established (mostly) transparent envelope systems that employ a ventilated cavity to either prevent or reduce the solar-induced cooling load or to passively exploit solar energy for solar heating purpose [1]. DSFs are usually classified as naturally ventilated or mechanically ventilated, where the latter, following the definition of mechanical ventilation in EN 12792 standard [2], have cavities ventilated by powered components, most often fans, that generate the airflow. In these systems, it is possible to assume that most, if not all, of the airflow rate through the DSF's cavity is not induced by naturally driven mechanisms. The fan-induced airflow rate can thus be considered an independent, controllable variable that can be employed to influence the performance of the DSF.

The mechanical ventilation of the cavity offers higher flexibility than a naturally ventilated DSF, which largely depends on stochastic and unpredictable external conditions. Natural ventilation in the cavity is sometimes dominated by thermal buoyancy [3] while at other times it is driven by wind [4,5], and very often, neither of these two factors can generate significant airflow [6]. Furthermore, prediction of the naturally induced airflow is far from trivial, making the control of this type of DSF much more challenging. In contrast, natural ventilation of the DSF's cavity is a solution that requires fewer components and possibly lowers maintenance, making it a suitable option when the priority is to reduce electrical energy use for air movement.

Therefore, the main reason for designing and operating mechanically ventilated double skin façades is to ensure (and control) the behavior of such envelopes by manipulating the cavity airflow, even if this comes at the cost of energy use for air movement.

E-mail address: francesco.goia@ntnu.no (F. Goia).

Nomenclature

Symbols

A	Area [m^2]
c	Specific heat capacity [Jkg^{-1} ^{o}C^{-1}]
g	Solar factor, g-value [-]
I	Solar irradiance [Wm^{-2}]
$\dot{m}$	Air mass flow rate [kgs^{-1}]
q	Heat flux density, heat flux rate [Wm^{-2}]
t	Temperature [^{o}C]
U	Thermal transmittance, U-value [Wm^{-2}K^{-1}]
V	Airflow rate / Normalised airflow rate [m^{3}h^{-1}]; [m^{3}h^{-1}m^{-1}]
γ	Dynamic insulation efficiency [-]
η	Preheating efficiency [-]

Subscripts

cav	refer to cavity
e	refer to exterior/outside
exc	refer to gained/released heat by the airflow passing through the cavity
exh	refer to the exhaust
hfm	refer to heat flux meter
i	refer to inside
ii	refer to the inner side of inner glazing

in	refer to the incident
inl	refer to the inlet
net	refer to net gain/loss
p	refer to constant pressure
tr	refer to transmitted
vent	refer to convective heat exchange between the indoor environment and freshly supplied air

Acronyms

ACH	Air change per hour
AHU	Air handling unit
ANOVA	Analysis of variance
DOE	Design of experiments
DSF	Double skin facade
FFD	Full factorial design
HE	Heat exchanger
HVAC	Heating, ventilation, and air conditioning
OFF	Not present blinds
RQ	Research question
RSM	Response surface methodology
SHTC	Surface heat transfer coefficient
UFM	Ultrasonic flow meter
VPM	Velocity profile method

The mechanically induced airflow can, if properly managed, positively impact the thermal and energy performance of a DSF. Among the most commonly adopted operational modes for these systems are the so-called *outdoor air curtain*, which aims at removing (solar) heat accumulated in the cavity [7], which is usually employed in the summer season or in predominantly hot climates, and the so-called *supply-air* façade, which instead exploits solar heat through the mechanical air flow rate to preheat fresh air for ventilation purposes [8], and is usually employed in winter or midseason, and particularly in cold-dominated climates. When a shading system is installed in the ventilated cavity, the interaction between this device and the ventilation flow rate deserves a comprehensive assessment to unveil how their interplay impacts the performance of the DSF.

The literature is rich in studies that explore the performance of DSFs under different conditions and configurations [9]. Previous studies have shown the significance of mechanical ventilation in relation to the supply of fresh air and the removal of excess heat from the cavity. Furthermore, previous research has also shown the impact of shading devices on the thermal performance of DSFs, and that venetian blinds are the most flexible in controlling the flow of heat and mass. However, a systematic investigation on how these two most important features interact in controlling the thermal and fluid-dynamics behavior of a DSF is a current gap in the literature. Only one experimental study in a controlled environment has been performed so far, in which the mechanical ventilation rate and the configuration of the venetian blinds were systematically altered [10]. However, only the efficiency of the façade in removing excess heat from the cavity was examined with a broad sampling of mechanical ventilation rates, leaving some relevant operational modes underexplored and impacts of different performance parameters unassessed.

1.2. Research significance, research questions, and structure of the paper

In the research presented in this paper, we systematically examined the possibilities of the combined effect of mechanical ventilation and shading device (venetian blinds) in utilizing the heat collected in the cavity. Two primary applications were considered based on their typical (expected) use, i.e., outdoor air curtain during the cooling season and supply air during the heating season. The novelty of this research lies in the detailed analysis and high-quality experimental data on the interaction between mechanical ventilation rate and operation of venetian blinds obtained by measurements in a climate simulator. The mechanical ventilation rate was sampled with small steps in a wide range, with a special focus on low airflow rates, which can be very important as the effects of this parameter and its interaction with the venetian blinds may not be trivial. The influence of ventilation rates and blinds on a series of performance metrics was analyzed, among them the preheating efficiency and the dynamic insulation efficiency. Experimental data collected during this research was made publicly available for further analysis and studies on DSF behavior, or for verification of numerical models [11].

The research questions that motivated us to perform the study are:

RQ1) *What is the impact of mechanically induced ventilation rate and venetian blinds on the thermal behavior of single-story DSF in typical conditions for warm winter and summer?*

RQ2) *In what way does mechanical ventilation interact with venetian blinds when it comes to the utilization of accumulated heat in a cavity?*

The results of this study can be significant for researchers dealing with the optimization of DSFs through seeking the most effective combination of mechanical ventilation rate and the shading setup for various purposes, such as the delivery and preheating of fresh air or reliving excess heat from the cavity. As described in more detail in the following sections, we selected a particular structure for the two glazed skins of our experimental mock-up that aimed at maximizing the exploitation of the solar energy by a DSF through the cavity ventilation. This choice, together with other fixed boundary conditions set to carry out the experimental analysis, may have had an impact on the magnitude of some of the assessed phenomena. However, we are confident that the response curves for performance indicators that we obtained for our specific

case study should show very similar functional dependence for all other DSFs of this type (single-story mechanical DSF with venetian blinds) and similar conditions to those that were tested, meaning that the validity and relevance of the findings of this study expand beyond the specific DSF construction employed in the measurements.

Beyond the introduction section of the paper, where we have scoped the research and specified the study's goal in the form of research questions, there are five additional sections. In Section 2 we summarize the current state of knowledge. This is followed by the sections in which the methods, results, discussion, and take-home lessons and conclusive remarks are presented. In Section 3 we briefly describe the experimental testbed and climate simulator, experimental design and boundary conditions, performance indicators, data analysis, and processing. The results are presented in Section 4 through a) the quantification of the overall impact of mechanical ventilation and venetian blinds on the thermal behavior of the DSF and b) the analysis of the combined effect of these two factors on the utilization of the cavity heat. In Section 5, Discussion, we reflect on the limitations and challenges of carrying out the experiments presented in this paper, and how the experimental design choices may have influenced the generalizability of the findings. In the last session, the main take-homes of this study are summarized and coupled with conclusive remarks, which also address possibilities for future research that can expand (and overcome some limitations of) the current study.

2. State of the art

The influence of mechanical ventilation and its combined effects with other construction elements on the thermal performance of DSFs has been the subject of interest in a number of studies. These studies have shaped our current understanding of the performance of such systems under different operational modes, which are deeply connected to the functional link between the DSF and the ventilation plant of the building. Oftentimes, mechanically ventilated facades are, in fact, deeply connected to the general ventilation concept of the building, and their degree of interaction with other components of the HVAC plant – such as the air handling unit (AHU) or simply an heat exchanger (HE) – can differ and lead to substantially different operational modes [8].

When the façade is designed to operate in the so-called *supply-air* mode, air pre-heated through the façade can either be injected directly in the room or sent to a local/centralized AHU or HE to further treat the air before it is supplied to the room. In this application, the DSF acts as a pre-heating device to reduce the ventilation sensible heat load. Conversely, when the focus is placed on the façade as a tool to reduce solar gain, its design operation falls in the category of an *outdoor air curtain* (if the cavity receives air from the outdoor environment) or of a *climate façade* (if the cavity receives air from the indoor environment – a case that has not been explored in this study). In both cases, the airflow through the façade is not meant to be supplied to the indoor space but can either be discharged to the outdoor or the solar heat gained by the airflow can be extracted by means of heat exchanges for other uses than compensating the ventilation load – hence transforming the façade into a sort of air-based solar collector.

As anticipated, mechanical ventilation can be beneficial in warm periods by reducing solar energy absorbed by a DSF, removing excess heat accumulated in the cavity, and lowering solar heat gains into the interior [12,13]. In such cases, an outdoor air curtain ventilation method is effective, where air enters from outside and passes through the cavity, absorbs heat, and increases in temperature. Finally, it leaves the channel through an outward-facing opening, redirecting a certain amount of the heat accumulated in the cavity toward the outside. Dynamic insulation efficiency has proved to be a good indicator of how well ventilation (in this case, mechanical) can remove heat accumulated in the cavity of the DSF and reduce overheating risk [14]. Mechanical airflow lowers the temperature of DSF structural elements by absorbing heat and thus reduces exchanged long-wave radiation [15]. However, sometimes in hot and sunny conditions, even high mechanically induced airflow rates cannot prevent overheating of structural elements. For example, in the case of the upper-crossed lateral ventilation scheme, the dynamic insulation efficiency is independent of the ventilation rate when there are venetian blinds in the cavity with almost closed slats (greater than 75°) [15]. When mechanical ventilation cannot prevent overheating, the operating costs of the fan become significant [16], such as in the case of a DSF with internal double glazing and an outer clear glass pane that is ventilated with an outdoor air curtain. In such cases, attention must be paid to passive ways to avoid overheating, such as adjusting the shading device or airflow path according to preferences [14].

Electrical energy use to power fans can also be increased due to other factors, such as a sharp-edged opening that behaves as an obstacle to the flow and creates recirculation zones near the inlet [17]. Reduction of width opening lowers the average velocity within the cavity and thus may affect fan's electricity consumption [18]. Increased turbulence can also lead to higher pressure drops [19], which in turns lead to higher energy use to power the fans. The shading device also influences mechanical airflow in the cavity by forming two channels, and if the flow is driven by the fans only, higher velocities will be encountered in the larger channel [20]. However, velocity distribution can be quite different when the flow is additionally driven by the thermal or wind effects [21]. The blind position in terms of distance to the glazing impacts air velocity and surface heat transfer coefficient (SHTC) more than the slat angle [21]. In the cavity where venetian blinds are installed, the airflow has highly complicated three-dimensional patterns, while the mean thermal field can still be considered two-dimensional in a vertical plane perpendicular to the glazing [22]. Forced flow through the DSF cavity mainly occurs in the thermally and hydrodynamically developing phase, meaning that it is characterized by higher SHTC than if it is fully developed [17]. However, in mechanically ventilated DSFs, just like in naturally ventilated, the primary role of the shading device is to control solar and visual gains [23]. Through flexible control of the shading state, which impacts on the transmitted solar radiation [24], venetian blinds allow one to adjust the desired level of daylighting inside the interior. Venetian blinds might not always be so effective in controlling glare, unless slats are placed in a completely closed position. Previous research on mechanically ventilated double-skin façades in hot and humid climates has shown, however, that even with fully closed blinds, sufficient daylighting conditions can be met when facades are exposed to direct sunlight, thereby minimizing solar heat gains and glare discomfort risk without compromising sufficient daylight levels [25].

One of the main advantages of DSFs compared to traditional single-skin envelopes in terms of thermal and energy performance is provided in the winter, as they can deliver a sufficient amount of preheated, fresh air by utilizing the greenhouse effect in the cavity [26]. In such configurations, the cold air enters the channel from the outdoors, warms up and rises, and if the greenhouse effect is pronounced, leaves the cavity to the interior sufficiently heated. For narrow cavities (∼10 cm), single float glass on the inner side leads to more intensive preheating than if double glazing is installed [27]. Also, the higher absorptivity of single-layer internal glazing will lead to greater heat exchange between the forced airflow and the glass, and consequently to greater preheating [28].

As mentioned, cavity-integrated shading systems (usually roller screen or venetian blinds) are an important component in many

DSFs as they allow control of both solar and luminous gains. These systems thus heavily influence at the same time the amount of solar heat absorbed in the cavity and the (direct) solar gain that reaches the indoor space; they are also functional in controlling the amount of daylight available in the indoor space, and in mitigating glare discomfort risk.

From a luminous perspective, the behavior and impact of screens or blinds in DSFs does not differ from the well-investigated behavior of these systems in combination with more traditional transparent components (e.g., a conventional single-skin curtain wall façade). However, the interaction between these systems and the cavity airflow is less trivial, as previously mentioned, and has been more widely investigated in the literature. Aluminum venetian blinds lead to a higher air preheating efficiency than a PVC reflecting roller screen due to the higher amount of absorbed solar radiation and the heat exchanged between the airflow and shading device [8]. Preheating can be enough to enable heat recovery and supply a sufficient amount of fresh air, which is very important for indoor air quality [26,29]. However, some investigations show preheating is not enough for most of the heating season, although these findings relate to a study in which a DSF was used as the exhaust outlet of the heating, ventilation, and air conditioning (HVAC) system, where the air was drawn from the interior of the room [14] – hence working as a *climate facade* according to the Belgian Building Research Establishment (BBRI) classification. Therefore, for a DSF to act as an energy-efficient solar exploitation system and contribute to airflow heating through the cavity rather than cooling, it is necessary to monitor the temperature of the exhausted air from the façade to decide whether to use it in combination with a heat exchanger [8].

3. Methodology

This research assessed the thermophysical behavior of a mechanically ventilated DSF by deliberate variation of mechanical ventilation rate and venetian blinds configuration in response to boundary conditions replicated by a climate simulator. The following methodological approach was devised to achieve the goals of this investigation. The research can be broken down into the several steps described by the following objectives:

1) To develop and equip an experimental testbed suitable for such investigation.
2) To select the appropriate experimental design and boundary conditions.
3) To identify performance indicators and carry out a series of experimental runs.
4) To analyze and post-process data in order to:
   a) quantify the impact of mechanical ventilation and venetian blind configuration on the thermal behavior of single-story DSF in typical winter and summer conditions;
   b) assess the combined effect of these two factors on the utilization of the cavity heat.

An experimental testbed developed in the previous research was upgraded and later employed for a series of experimental tests in a climate simulator. Basic information on the tested DSF configuration can be found in the subsection below, but a more detailed description of the experimental testbed is provided in a dedicated publication [30].

3.1. The experimental testbed

3.1.1. The DSF mock-up and system for measurement

A full-scale DSF mock-up equipped with more than 70 sensors and a system for monitoring and controlling the experiment was employed for systematic investigation in a climate simulator. A series of experiments involved altering only mechanical ventilation rate and venetian blind setup, while all other construction features were held constant. A 200 mm cavity separates the inner and outer glazing of the test element with installed venetian blinds colored in white aluminum with an estimated reflectivity between 0.5 and 0.6 [31]. The same glazing covers both sides of the test element, and it consists of 4 mm thick double glazing separated by the 15 mm gap filled 90 % with Argon and 10 % with air. A cavity is connected through the upper opening with a system of ducts (radius of 20 cm) with a fan capable of generating an airflow rate up to 1000 m³h⁻¹ (Fig. 1). The fan causes a pressure difference that forces the air to enter the cavity from the lower opening on the outer side of the DSF (air is drawn from the outdoor chamber). After passing through the cavity, the air exits through the upper opening and reaches the fan through connected ducts. Finally, it is discharged into the inner or outer chamber, depending on the desired flow path (Figs. 1 and 2b). The fan employed in the testbed is an axial impeller (a rotor placed in a duct) with curved blades that can produce a maximum flow rate of 271 ls⁻¹ (976 m³h⁻¹). The nominal flow rate of the fan is 0.115 m³s⁻¹ (414 m³h⁻¹), while the nominal external pressure is 397 Pa. For the developed experimental setup, the highest airflow rates that the fan could produce at maximum power measured by the ultrasonic flow meter were in the range of ∼865 – ∼890 m³h⁻¹.

The airflow rate in the cavity was assessed by the velocity profile method (VPM) and ultrasonic flow meter (UFM). Twelve hot wire anemometers were arranged along three heights (¼, ½, and ¾ of glazing height) to measure the velocity of the air (Fig. 2a). The values of the airflow rates were obtained from the second and third heights, while the values from the first level were discarded due to the dissonant readings from two hot-wire anemometers, which were likely to be either poorly performing sensors or affected by unidentified disturbances. The final value was obtained by averaging the values from these two heights. Measurements with the ultrasonic flow meter were performed in the duct that was connected with the cavity through the upper opening and ventilation system (Fig. 2b). Target irradiance value on the façade was measured using one spectrally flat, class B pyranometer [32] placed at the center of the glazed area of the DSF. However, the solar irradiance distribution on the outer DSF surface was also assessed using five photovoltaic pyranometers evenly distributed to obtain a more detailed picture of actual values at different surface points (Fig. 2b). Though less accurate, these photovoltaic pyranometers were verified against the thermopile and showed a deviation of up to 4.5 %.

Although over 70 sensors were mounted on the DSF mock-up, Fig. 2 shows only the most important ones used in this experimental campaign for clarity and readability. The temperature of the glass pane facing the indoor chamber was measured at three heights, the same as the hot-wire anemometers, using four surface temperature sensors. Two heat flux meters were placed on the same glass pane to measure the heat flux density toward/from the interior space, where the representative value for the whole DSF glazing was obtained by averaging these two values. The air temperature near the inlet was measured using four air temperature sensors. The air temperature near the upper opening, to which the ventilation system was connected, was measured in the same way. All temperature, heat flux and air speed sensors were shielded from the effect of (artificial) solar irradiance using well-established practices and methods.
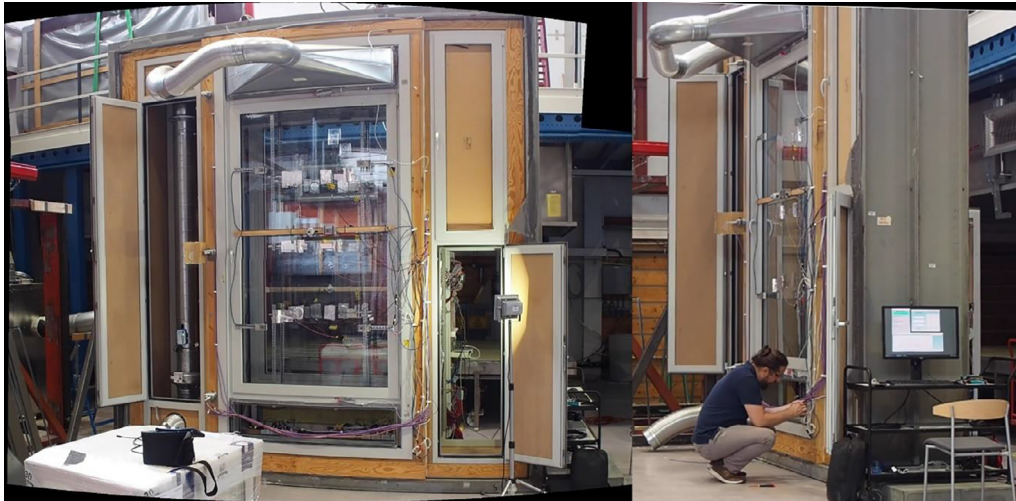
Fig. 1. The DSF draws air from the lower opening and transfers it through the cavity to the upper opening. Further, the ventilation system attached to the upper vent takes the air first to the ultrasonic flow meter and then to the fan located in the vertical duct placed in the DSF's side section. Finally, the air is expelled to the outside or inside as needed.
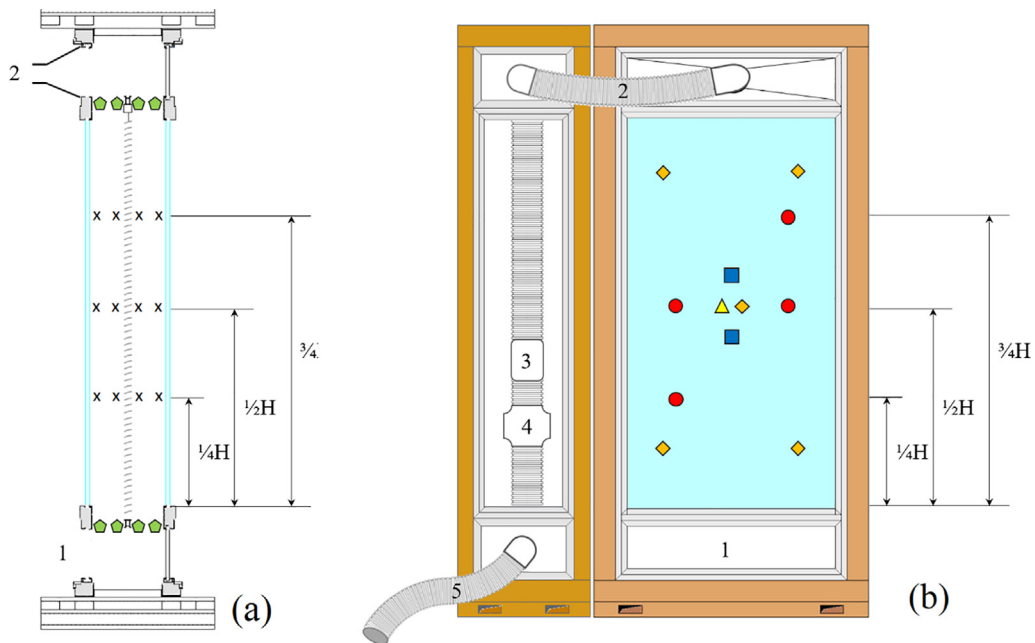

Fig. 2. a) Layout of sensors in the cavity, b) Layout of sensors placed on the indoor glazing, and a sketch of the ventilation system attached to the DSF. Labels meaning: X – hot wire anemometers, ⬠ - air temperature sensor, □ – heat flux meter, △ – thermopile pyranometer, ◇ – photovoltaic pyranometer, ○ - surface temperature sensors, 1 – inlet, 2 – ventilation system attached to the upper opening, 3 – ultrasonic flow meter, 4 – fan, 5 -exhaust.

3.1.2. The climate simulator

The climate simulator facility consists of two chambers intended to replicate indoor and outdoor conditions in terms of temperature and humidity. The outdoor chamber contains a solar simulator that can emit a radiation with a spectrum similar to that of solar radiation, with an intensity up to 1000 Wm^{-2}. The equipped DSF mock-up is placed between two sections and subjected to different boundary conditions in the two chambers.

3.1.3. Measurement of the airflow rate

Since both methods for airflow assessment (VPM and UFM) had drawbacks, a combined profile of airflow rate was used to calculate indicators of fluid-dynamics behavior. The UFM measurements were used to fit the lowest part of the airflow rate profile (up to 15% of maximum fan power), while the values obtained by the

VPM were used for the upper part so that each of the two methods was considered in the range where it delivered the best performance and was free from intrinsic (sensor limitations) or extrinsic (installation limitations) shortcomings. In order to obtain a unique and smooth profile with no clear transition between UFM and VPM measurements, discrete measurements were fitted to a third-order polynomial function. The measured airflow rates were normalized by the facade width (1.4 m), and this ventilation rate value will be presented later in the paper.

3.2. Experimental design and tested boundary conditions

This experimental campaign focused on understanding the influence of structural factors in clearly defined conditions, and therefore this study did not include an assessment of the effect

of environmental factors alone on the thermophysical behavior of the DSF. The flexible mock-up allowed testing of a large range of configurations through modifications of the venetian blind setup and mechanical ventilation rate. Venetian blinds were placed in three configurations: closed (0°), half-opened (45°), and not present (OFF), while the mechanical ventilation rate was controlled through a percentage of maximum fan power. Since the focus was on a more detailed analysis of the impact of mechanical ventilation, a higher-than-usual number of levels were selected for this factor (0, 10, 15, 20, 30, 40, 50, 75, and 100%). Therefore, experimental designs such as Taguchi, definite screening, and arrays related to the response surface methodology (RSM) were dropped [33], and full factorial design (FFD) was selected as appropriate. In a FFD, a series of experiments encompass all possible combinations of chosen factors and levels, consisting in this case of 27 experimental runs. However, for summer boundary conditions, due to technical limitations, a level corresponding to 75 % of maximum fan power consumption was omitted from the analysis, and therefore that series consists of 24 experimental runs (Table 1). According to our assumptions, which were later confirmed in the results, this point was not important from the aspect of analysis since, for the highest air flow rates, the indicators of thermal behavior did not change significantly.

In a previous study [31], the design of experiments (DOE) methodology was employed to assess the thermophysical behavior of a DSF for a wide range of summer boundary conditions. In this way, apart from the influence of structural elements, the impact of environmental parameters was quantified. However, by choosing a wide range of boundary conditions, a wide range of variations of behavioral indicators was obtained as well, thus including a large number of situations in which the impact of construction elements on response quantities was either not necessary or it was negligible. Accordingly, the impression was that the influence of the construction features was modest, but actually, it was masked by the impact of environmental parameters. Therefore, in this experimental campaign, the effect of environmental parameters was not examined in order to gain a better insight into the influence of construction elements on the thermal and fluid-dynamic behavior of DSF. Fixed boundary conditions were selected for "problematic" situations where the intervention of operational modes is needed to influence the thermophysical behavior of the DSF.

For the analysis of the utilization of excess heat accumulated in the cavity and prevention of DSF overheating, boundary conditions corresponding to g-value calculation were selected [34], which are more or less typical for summer conditions. Those were outdoor and indoor temperatures, 30 ℃ and 25 ℃, respectively, and solar irradiance of 500 Wm^{-2}. Such conditions correspond to the warm summer day, where a lot of heat accumulates in the cavity due to not enough strong naturally-generated airflow capable of removing this excess heat [31]. In this way, a better insight into the effect of mechanical ventilation and its interaction with shading as the most influential structural element can be obtained for situations when natural ventilation cannot expel excess heat from the cavity.

For the analysis of air preheating in the DSF cavity, the boundary conditions corresponding to typical situations for air preheat-

ing (cold outdoor air and low-to-moderate solar irradiance) were selected. Due to the limitations of the climate simulator, we went to the limit of its capabilities: the lowest possible temperature during the active solar simulator and the minimum achievable solar irradiance. These were around 10 ℃ and 300 Wm^{-2}, respectively, while for the indoor environment, a temperature of 25 ℃ was selected in order to establish a greater temperature difference between interior and exterior. We believe that the selection of higher internal temperature compared to the typical 20 ℃ for residential buildings or for office spaces during the heating period did not affect the functional dependence of performance indicators on construction features. After all, it is neither the internal nor the external temperature level alone but the temperature difference that drives physical processes, such as heat and mass transfer – and within a relatively close change in temperature levels the assumption of linearity in the thermal and fluid mechanics processes is fully reasonable.

3.3. Performance indicators

The following quantities were chosen for performance indicators of thermal and fluid dynamics behavior: net heat flux density (q_{net}), dynamic insulation efficiency (ε), air preheating efficiency (η), average cavity temperature (t_{cav}), g-value (also known as solar factor, solar heat gain coefficient, or total solar energy transmittance), the indoor surface glazing temperature (t_{ii}), and the heat gain rate by the airflow (q_{exc}). The net heat flux density represents the sum of measured heat flux density by the heat flux meter and transmitted solar radiation intensity measured by the pyranometer set behind the inner glazing in the indoor chamber. In the case when the air is delivered from the outside to the interior through the cavity, this quantity is supplemented by the convective heat exchange between the indoor environment and freshly supplied air (q_{vent}). This latter qauntity represents the heat flux density that needs to be absorbed or released by the imported air in order to bring itself into thermal equilibrium with the indoor environment. The dynamic insulation efficiency [14] represents the portion of the heat flux entering the cavity from the outer side that is removed and directed back by the airflow toward the outside. This quantity is a very important indicator of the ability of a DSF to relieve its cavity from excess heat by ventilation in hot periods.

The preheating efficiency represents the ratio of two temperature differences, where the one in the numerator represents the difference between the temperature of the air delivered to the indoor space and the exterior temperature. The denominator indicates the difference between the air temperatures in indoor and outdoor spaces. The preheating efficiency measures the capability of the DSF to preheat the ventilation airflow rate during the cold season [35]. The equation for the preheating efficiency given in Table 2 is derived from a somewhat more general formula that includes air preheating in other situations as well [8,36], such as air preheating when the air is drawn from interior space or when the air is not used for direct ventilation but goes through additional preheating.

Table 1
Selected factors, levels and boundary conditions.

Factors	Levels								
Fan rate [%]	0	10	15	20	30	40	50	(75)	100
The venetian blind setup [°]	OFF (not present)				45		0		
Tested boundary conditions	Temperature [℃]				Solar irradiance [Wm^{-2}]				
Summer	30				500				
Mid-season/Winter	10				300				

The average cavity temperature was obtained from temperature measurements of 12 hot-wire anemometers using a volume-weighted average. Solar factor (g-value) was evaluated based on the ratio between the measured net heat flux density and the incident solar radiation on the outer side of the DSF using the method for non-calorimetric assessment of in-situ solar factor of glazed systems [45]. The indoor surface glazing temperature represents the temperature of the inner glazing surface facing the indoor environment, and it is calculated as the area-weighted average of four-point measurements. The heat gain rate by the airflow represents the heat rate absorbed by the airflow passing through the cavity normalized by the DSF surface. It is calculated based on the evaluated airflow rate and measured temperature gain of the airflow through the cavity. Temperature difference refers to the difference between exhaust air and inlet air temperatures. The outdoor temperature could also be used instead of the inlet air temperature because the values of these two quantities are almost identical.

To calculate ventilation rates to check the requirements given by the standard EN 16798 [37,38] in terms of indoor air quality and delivery of sufficient quantities of fresh air, we assumed an office with a depth of 5 m behind the DSF and a height of 3 m. This assumption means that behind each DSF module with a 1.5 m width, an air volume of 22.5 m³ and a floor area of 7.5 m² were associated with each façade module. According to the EN 16798 standard [38], the floor area occupied by one person in the single and landscape office is 10 m² and 15 m², respectively. Therefore, it was assumed that only one person occupies the space located behind the DSF. Minimum ventilation rates per person for offices (single and landscape) range from 2.5 to 10 ls⁻¹person⁻¹, depending on the environmental quality category (from low to high). If these values are converted into more familiar forms of ventilation rates, then they will amount to 9 – 36 m³h⁻¹ (expressed in cubic meters per hour), ~7 – ~26 m³m⁻¹h⁻¹ (normalized by the glazing width), and 0.4 – 1.6 ACH (air changes per hour).

3.4. Data analysis and processing

After performing a series of experimental runs according to the FFD, the experimental data were collected, and the analysis of variance (ANOVA) was performed over two data sets, which referred to two typical situations (winter/mid-season and summer). The influence of mechanical ventilation rate and venetian blind configuration on the thermal and fluid-dynamics behavior was represented through contributions of each factor on the variance of the behavioral/performance indicator. The contributions of mechanical ventilation rate and venetian blind setup (c_{MV} and c_{VB}) were calculated as the ratio of the sum of squares for these factors (SS_{MV} or SS_{VB}) and the total sum of squares (SS_T):

$$c_{MV} = \frac{SS_{MV}}{SS_T} 100 \; and \; c_{VB} = \frac{SS_{VB}}{SS_T} 100$$

Table 2
Description of performance indicators.

Performance indicator	Unit	Equation
Net heat flux density	[Wm⁻²]	$q_{net} = q_{hfm} + I_{tr} + \frac{\dot{m}c_p(t_{exh}-t_i)}{A}$
Dynamic insulation efficiency	[-]	$\gamma = \frac{\dot{m}c_p(t_{exh}-t_{inl})}{q_{hfm}A+q_{tr}A+\dot{m}c_p(t_{exh}-t_{inl})}$
Air preheating efficiency	[-]	$\eta = \frac{t_{exh}-t_e}{t_i-t_e}$
Average cavity temperature	[°C]	$t_{cav} = \frac{\sum_{n=1}^{16}t_{cav,n}}{16}$
g-value	[-]	$g = \frac{q_{net}}{I_{in}} = \frac{q_{hfm}+I_{tr}}{I_{in}}$
The indoor surface glazing temperature	[°C]	$t_{ii} = \frac{\sum_{n=1}^{4}t_{ii,n}}{4}$
The heat gain rate by the airflow normalized by the DSF surface	[Wm⁻²]	$q_{exc} = \frac{\dot{m}c_p(t_{exh}-t_{inl})}{A}$

where subscripts MV and VB refer to mechanical ventilation rate and venetian blinds setup/configuration, respectively.

An FFD with only two factors cannot assess the statistical significance of the interaction between these factors. One option would be to fold the FFD, i.e., duplicate the pattern of this design and carry out an experimental campaign twice, but since it would require extensive material resources, it was abandoned. Another option, requiring fewer resources, was to use some of the designs related to the response surface methodology or a folded Taguchi design. However, such an approach would require that the number of levels corresponding to the mechanical ventilation rate be reduced to 3 or 4, potentially losing more detailed insight into the effects of this factor. Nevertheless, the combined effect of mechanical ventilation rate and venetian blind setup was assessed directly from the graphs showing the dependence of the performance indicators upon these two factors. In order to obtain the dependence curve, a linear change was assumed between the points at which the response quantity was sampled according to the FFD pattern.

4. Results

4.1. Overall thermal and fluid-dynamics behavior of a mechanically ventilated DSF in specified conditions

In the tested winter conditions, the mechanical ventilation rate had prevalence over the venetian blinds in controlling the indicators of thermophysical behavior of the DSF, except for the solar heat gain coefficient (g-value) (Fig. 3). The amount of heat that the air supplied by mechanical ventilation exchanged with the internal environment represented the dominant component in net heat transfer. Therefore, the mechanical ventilation by controlling the amount of delivered air also controlled the net heat transfer. The forced air flow rate dictated the convective heat exchange between the air passing through the cavity and the surrounding borders and thus significantly affected the amount of heat absorbed by the airflow. The effect of the shading device was limited, most likely due to the low thermal capacity and high solar reflectivity of the blinds, together with a relatively low impinging solar irradiance. A combination of several factors most likely led to the reduced impact of the venetian blinds on the indoor surface glazing temperature. The amount of the absorbed radiation on the indoor-facing glass pane was quite limited due to three glass panes in front reducing the available radiation for absorption. Additionally, the relatively low absorption coefficient of these glass panes further decreased the amount of absorbed radiation, and thus its variations arising from the venetian blind setup. Consequently, the temperature of the indoor glazing was influenced more by the heat transferred by the mechanical ventilation than by the absorption of solar irradiance that the venetian blinds could control. Similarly, like for the heat gain rate by the airflow, mechanical ventilation rate was dominant in controlling the preheating efficiency. As expected, the shading device, through the control of transmitted solar radiation, took over the role of the dominant factor in the regulation of solar heat gain coefficient.

Unlike in the previous period, under summer boundary conditions and with the DSF operating in OAC, venetian blinds were more dominant than mechanical ventilation in controlling the thermophysical behavior of the DSF, except for heat gain by the airflow in the cavity and the dynamic insulation efficiency (Fig. 3). Since, in this configuration, the indoor air was isolated from the outdoor, the largest share of the net heat transfer belonged to the transmitted radiation, which is why the impact of venetian blinds was far more pronounced. It is to be expected that the identical causes (low thermal capacity of blinds and, especially, high solar reflectivity) as in the previous case made mechanical ventila-
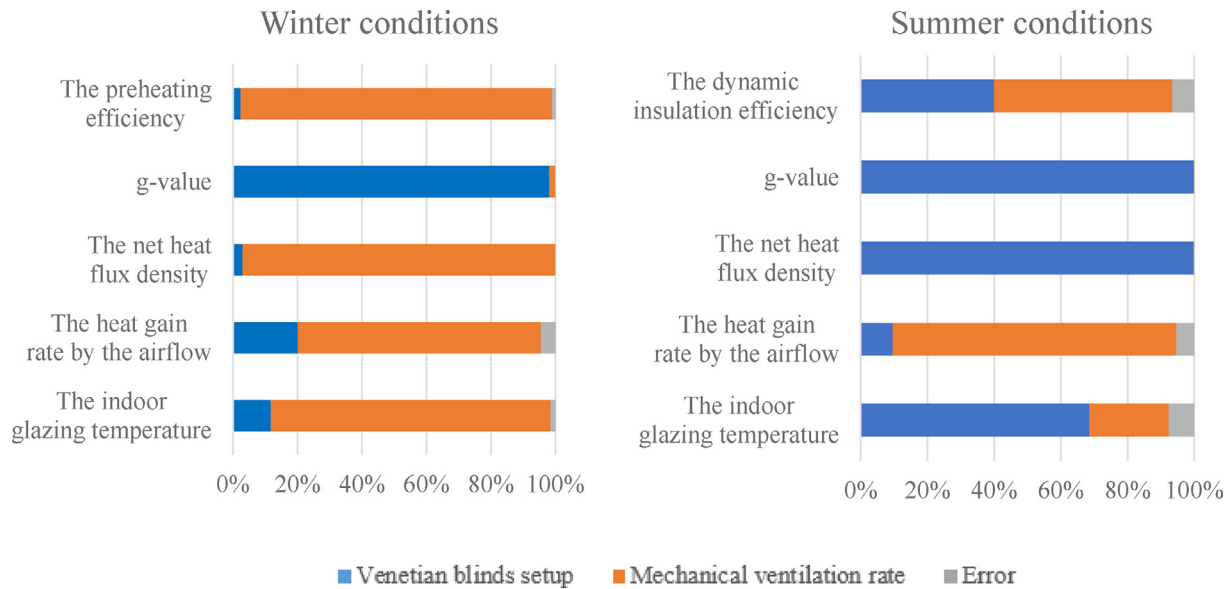
Fig. 3. The overall thermal and fluid-dynamic behavior of the mechanically ventilated DSF in winter (left) and summer (right) conditions.

tion significantly more effective than the shading device in managing the heat gain rate by the airflow. Both factors were almost equally important in driving the dynamic insulation efficiency. Compared to the winter conditions, the higher solar irradiance led to a more prominent role of venetian blinds in controlling the indoor glazing surface temperature. As expected, the value of the solar heat gain coefficient was managed efficiently with the shading device, while the influence of mechanical ventilation was minimal. This effect can be understood by comparing the magnitude of the energy flow linked to the cavity airflow with that of other energy flows across the façade, (Fig. 4). A somewhat higher value of unexplained variance in both the dynamic insulation efficiency and the indoor glazing temperature indicates the possible need for the addition of nonlinear terms to describe these quantities' behavior adequately.

4.2. The combined effect of the mechanical ventilation and venetian blinds

For a reference office with a depth of 5 m and a height of 3 m, low mechanical ventilation rates (up to 80 $m^3 m^{-1} h^{-1}$) would be enough to provide fresh air (up to 5 ACH) and sufficiently preheat the air (Fig. 5a) to compensate the ventilation sensible heat load and even contribute to space heating with ventilative heating – or potentially contribute to a cooling load, if there is no space heating load. However, any further increase in the airflow rate from these values (greater than 5 ACH) would significantly decrease the net heat flux density (i.e., the total heat gain due to surface heat flux, direct solar gain, and convective gain due to the airflow) because of the negative (cooling) convective gain through the airflow. Such an increase of the airflow rate (up to a value of about
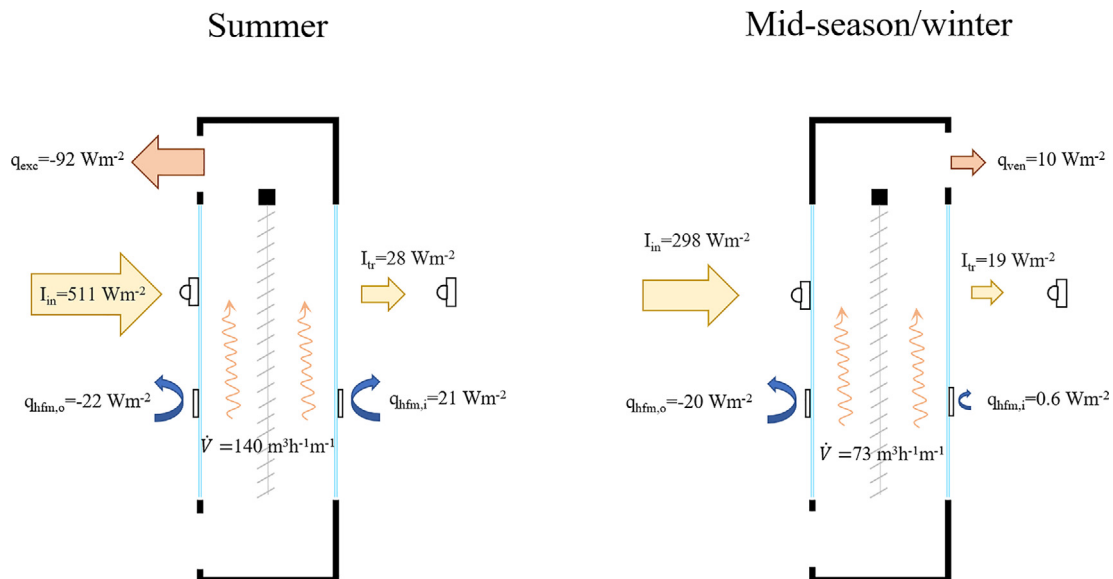

Fig. 4. Energy flow diagram in summer and mid-season/winter conditions (I_{in} and I_{tr} – incident and transmitted solar irradiance measured by the thermopile pyranometer, $q_{hfm,i}$ and $q_{hfm,o}$ – heat flux density measured by the heat flow meter installed on the indoor and outdoor glazing, $\dot{V}$ – airflow rate normalized by the glazing width, q_{exc} – heat flux rate absorbed and removed by the airflow rate passing through the cavity and q_{vent} – heat flux rate exchanged between the supplied fresh air and the indoor environment.
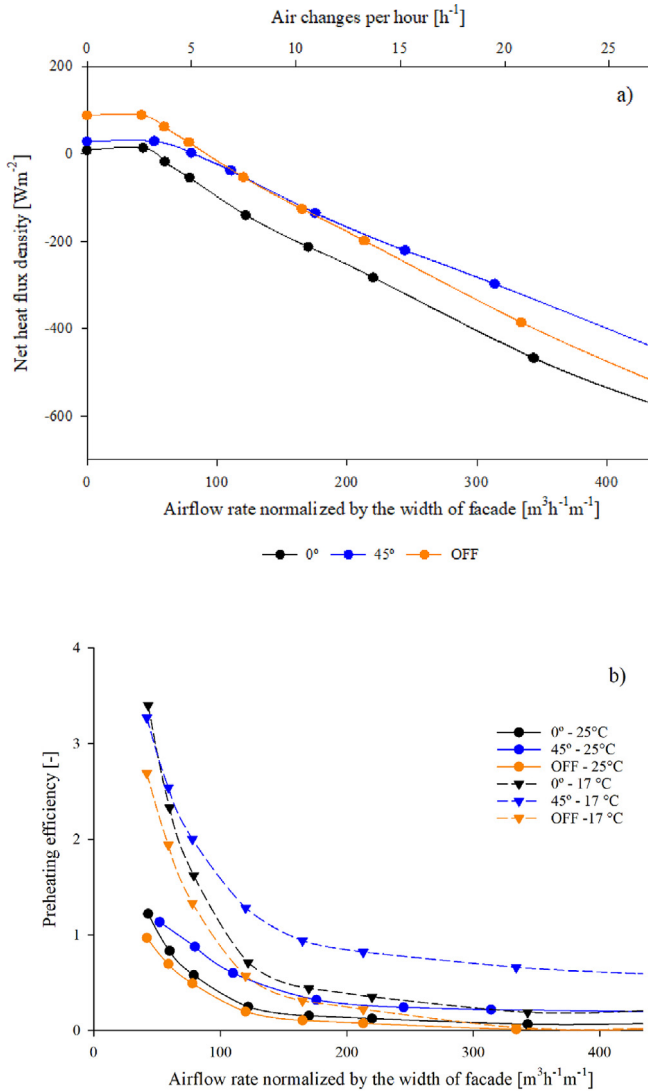
Fig. 5. The combined effect of mechanical ventilation rate and venetian blind set up on a) the net heat transfer and b) preheating efficiency (right) in the considered mid-season/winter conditions.

150 m^{3}m^{-1}h^{-1}) may nevertheless not be critical considering that in contemporary buildings with high insulation and airtightness levels, the interior gain may be sufficient to lead to cooling loads also in winter and mid-season.

For the same reason, preheating efficiency (with baseline 25 ℃) was around 1 [-] only for lower airflow rates, with a drastic reduction for higher rates. The mechanical ventilation could not even provide sufficiently heated air from the cavity if venetian blinds were raised, while its presence caused an increase in the preheating efficiency. In the considered boundary conditions, preheating efficiency was the highest when the blinds were semi-opened, except in a short interval for the lowest airflow rates, where the fully closed blinds led to the most intensive preheating. Fig. 5b shows the values of the preheating efficiency for a supply air temperature setpoint of 17 ℃. This value was chosen to represent the performance in terms of the ability to provide enough heat to the fresh-air airflow, which is oftentimes supplied to a room with a temperature below the room temperature setpoint. It is possible to verify that this target temperature can be achieved, depending on the exact configuration of venetian blind, with an airflow rate in the range of 80 to 150 m^{3}h^{-1}m^{-1}. The dependence on the airflow

rate of the preheating efficiency curves for this supply temperature clearly does not change significantly and they retain their basic characteristic of the curves related to the setpoint temperature of 25 ℃. When comparing the three shading configurations, with the slats entirely shut, the lowest ventilation rates (60 m^{3}h^{-1}m^{-1}) were required to reach a negative value for the net heat transfer, while in the absence of the blinds, it remained positive for airflow rates as high as about 80 m^{3}h^{-1}m^{-1}).

Under the considered winter conditions, the highest amount of absorbed heat by the airflow was found for low mechanical ventilation rates (50 – 80 m^{3}m^{-1}h^{-1}), where further increase first led to a slight decrease and then to stagnation of the absorbed heat (Fig. 6a). The slats in a semi-opened position (45°) transferred more heat to the airflow than completely closed slats, most likely due to increased turbulence and amplified heat transfer between slats and fluid. For low airflow rates (up to 60 m^{3}m^{-1}h^{-1}), airflow temperatures at the outlet of the cavity were more than ten degree
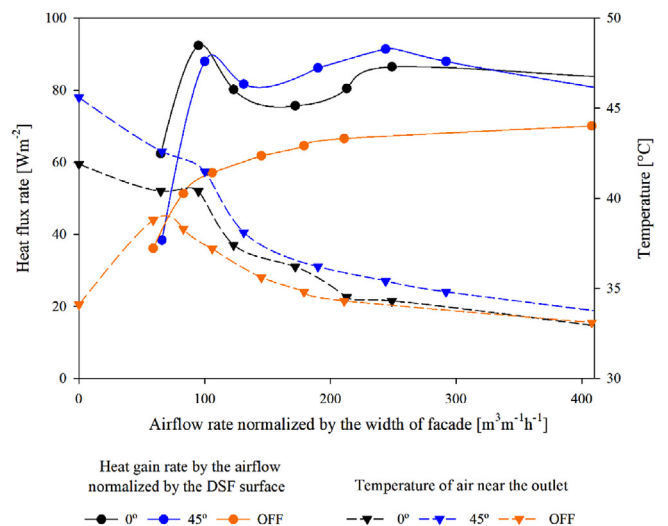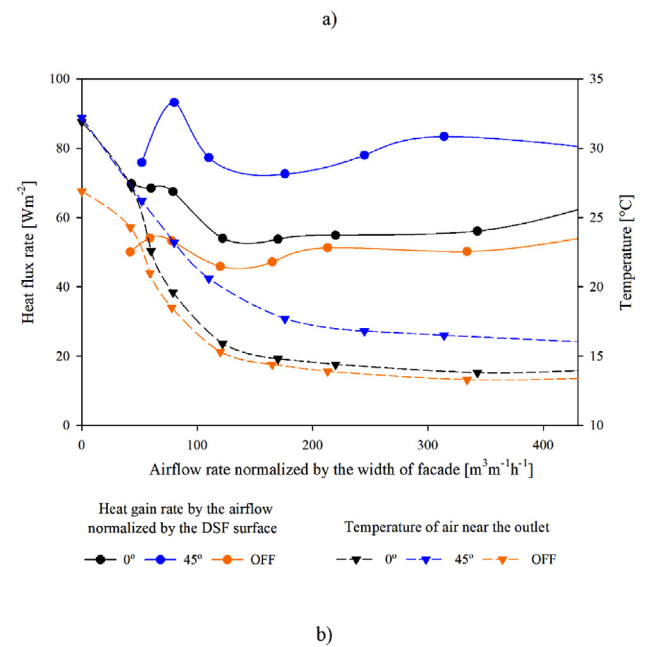
a)

b)

Fig. 6. The combined effect of mechanical ventilation rate and venetian blind setup on the normalized heat gain rate by the airflow and temperature of the airflow near an outlet in a) mid-season/winter and b) summer conditions.

Celsius higher than the outside air temperature. The curves describing the heat absorbed by the airflow in summer conditions are very much like those corresponding to the winter conditions, with similar values of the absorbed heat (Fig. 6b). The only difference was a somewhat more gradual increase in the heat absorbed by the airflow with the rise in the ventilation rate. The presence of blinds increased the amount of heat transferred to the airflow, but unlike in the tested winter conditions, there was no significant difference between the slats semi- or completely closed. In the case of lowered venetian blinds and airflow rates up to 100 $m^3m^{-1}h^{-1}$, airflow temperatures at the cavity outlet were over 40 ℃, indicating the potential of the DSF as a "solar collector," thereby allowing the excess heat accumulated in the cavity to be used for various purposes. The presence of mechanical ventilation did not always decrease the airflow temperature at the cavity outlet, as seen from the example when the venetian blinds were not lowered. For low ventilation rates (∼40 $m^3m^{-1}h^{-1}$), the air temperature near the exhaust is around 4 to 5 ℃ higher than when the fan is not active.

The average temperature of the indoor glazing in both considered representative situations shows similar characteristics: it is very close to 25 ℃ and was stable, which means it changed slightly with a change in the configuration of the venetian blind and the mechanical ventilation rate (Fig. 7a and b). This little dependence of the surface temperature on the boundary conditions was likely due to the selected interior skin glazing (a double glazed unit with

relatively low thermal transmittance). In the tested mid-season/winter conditions with no ventilation or at very low rates, the average temperature of the cavity became similar in the case of semi-opened and closed slats, while raising the venetian blind led to a decrease in temperature of a few degrees Celsius. However, in the presence of ventilation, the average cavity temperature in the case of closed blinds decreased and became closer to the cavity temperature without venetians. In such conditions, semi-open slats caused the highest cavity temperatures. The shading device had a higher temperature than the cavity, and that difference was more pronounced when the slats were closed. In the considered summer boundary conditions, the shading device reached temperature values above 40 ℃ in the case of closed slats, even for medium ventilation rates. Generally, the temperature of the shading device was higher than 35 ℃ for any ventilation rate, regardless of whether they were semi-opened or closed, indicating significant overheating. The mechanical ventilation rate may decrease the temperature value by up to 10 ℃, and this change was most noticeable for semi-opened slats. By increasing ventilation rates, the cavity temperatures in the case of different shading device setups converged towards one temperature, but as in the case of venetian blinds, they exceeded 35 ℃ for low and medium ventilation rates. Nonetheless, having an insulated unit (with a low-emissivity layer in the gap) as the inner skin greatly reduced the influence of the blinds' slat temperature on the radiative heat exchanges in the DSF, therefore making this variable of little interest when it comes to the risk of additional heat gain due to overheating of elements or air in the cavity.

In the tested configuration, typical for a summer period where the indoor environment was decoupled from the outdoor, the blinds dominated the net heat transfer entirely. The effect of mechanical ventilation was minimal, as seen in Fig. 8b, where the net heat flux density curves are practically horizontal. As expected, the largest amounts of heat directed inwards were in the case of open slats and the least in the case of the closed. Fully risen venetian blinds are not recommended because they lead to excessive cooling load, while completely closed slats are, generally speaking, not very suitable to balance the thermal performance of the DSF with its daylighting performance – a domain that even if not investigated in this study is clearly an important variable in the global operation of a DSF and will be briefly considered in the Discussion section. The risk of overheating in summer conditions seems to be controllable and avoidable, as long as the façade is operated in an outdoor air curtain and shading devices are deployed. For example, for venetian blinds at 45° and a moderate airflow rate of nearly 150 $m^2h^{-1}m^{-1}$ (Fig. 4), the total gain through the façade under summer conditions was below 50 Wm^{-2} – for reference purpose, a conventional single skin façade with a window to wall ratio of 0.3, state of the art envelope systems, and glazing with a g-value of 0.2, would lead under the same tested condition to a heat gain in the range of three times that of the tested DSF. Unlike the net heat transfer, the mechanical ventilation significantly affected dynamic insulation efficiency up to a certain point (100 ∼ 150 $m^2h^{-1}m^{-1}$), corresponding to relatively low ventilation rates, after which further increase did not lead to any significant change (Fig. 8a). The influence of venetian blinds on the dynamic insulation efficiency was also substantial, where the closure of the blinds led to an increase in the dynamic insulation efficiency.

5. Discussion

Measuring thermophysical quantities is a process not free from uncertainty and complexity. The experimental testbed employed in this analysis consisted of tens of sensors and we encountered certain challenges that should be considered in assessing the out-
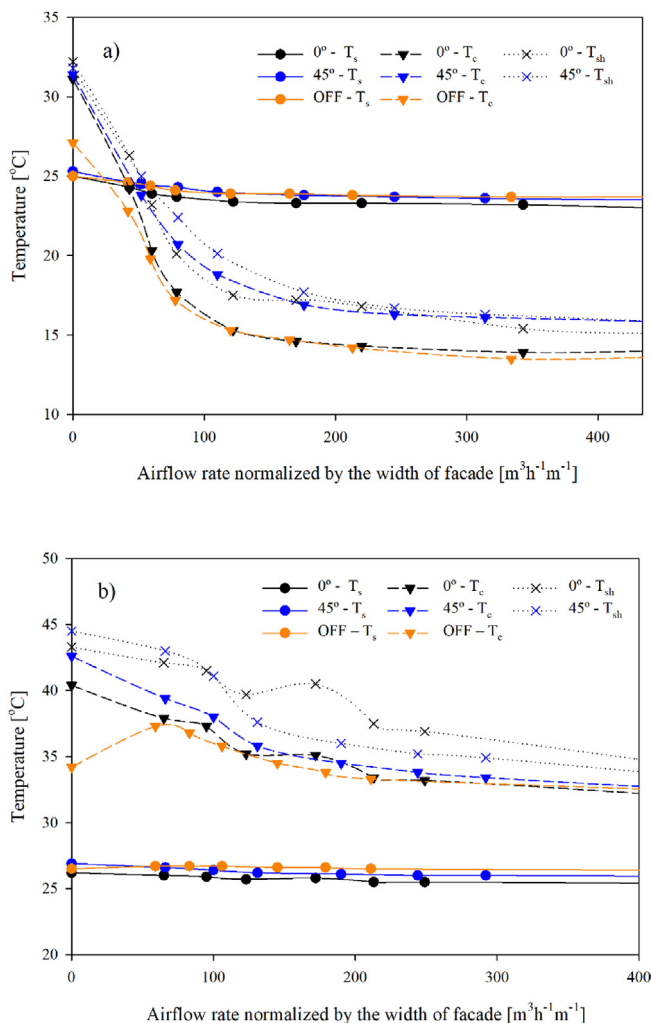

Fig. 7. Average temperatures of the indoor glazing (T_s), cavity (T_c), and shading (T_{sh}) in the a) mid-season/winter and b) summer conditions.
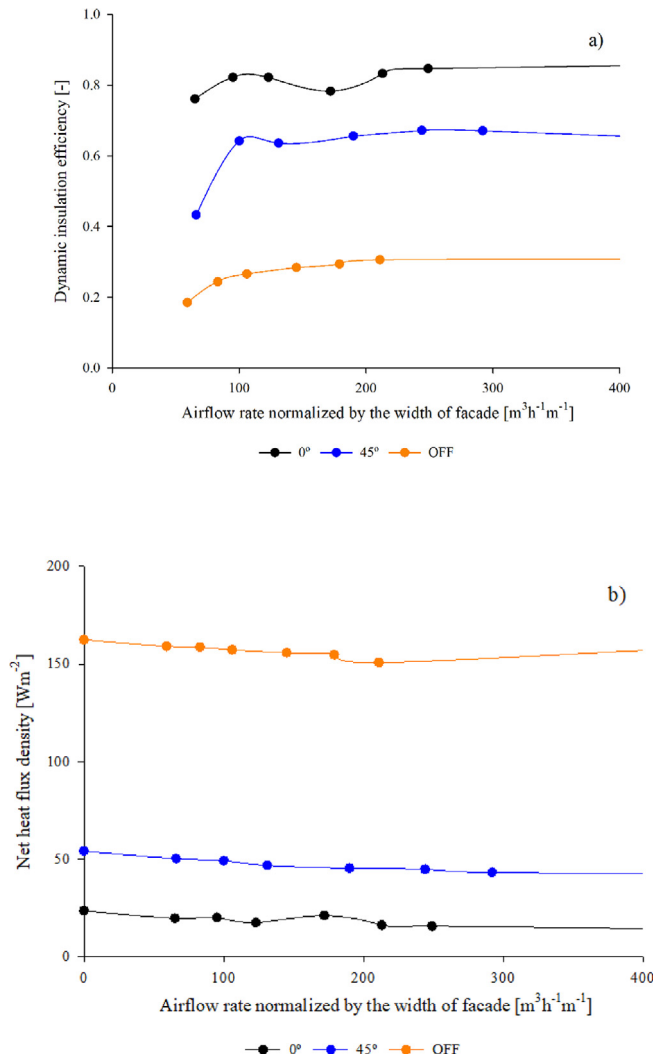
Fig. 8. The combined effect of mechanical ventilation rate and venetian blind set up on a) the dynamic insulation efficiency and b) net heat transfer (right) in the considered summer conditions.

put of the analysis just presented, as they may have an impact on the quality of the results. Similarly, carrying out experiments only requires selecting a series of boundary conditions and experimental design choices that also can impact the generality of the results.

One of the challenges we encountered was evaluating the air temperature near the exhaust, where we could not rely on measurements from the air temperature sensors located near the outlet (Fig. 2) due to unexpectedly low readings, likely influenced by heat exchanges outside the cavity. Instead, temperature measurements obtained from the hot-wire anemometers located on the 3rd height were taken as more representative for calculating the result of heating the airflow in the cavity in this study. The cause for these low readings was most likely air infiltration in places where the ventilation system is attached to the upper opening, and due to the features of the façade mock-up that made it a flexible platform to test many DSF configurations – which might differ from a "real," fixed-configuration DSF with properly fully insulated inlet/outlet section. Another reason could be the possible existence of a recirculation zone at the channel outlet [39]. This pattern might cause the mixing of the colder air from the opaque upper part of the cavity.

As stated earlier, the airflow rate profile was obtained using a combination of measurements from the VPM and UFM due to the limitations of both instruments and methods. Because of the lower

threshold limit typical of hot-wire anemometers, the VPM has problems determining the lowest airflow rates and their direction if the temperature differences are minor or mechanical and natural ventilation is present simultaneously [40]. Therefore, the ultrasonic flow meter measurements were more appropriate to measure the airflow rate profile corresponding to the lowest fan rotation rates. Due to a greater pressure difference and, possibly, insufficiently fully airtight sealing, higher rotation rates likely increased infiltration through joints of the ventilation system (especially the connection to the upper opening), even if measures were put in place to limit possible infiltrations along the airflow path. For that reason, the ultrasonic flow meter registered higher mass flow rates than the velocity profile method (Fig. 9). Thus, the values calculated by the VPM were more appropriate to measure the actual mass flow in the DSF cavity without overestimating it due to infiltrations that might have happened at connection points in the ducts outside the façade. Since the temperature difference is not a reliable indicator of airflow direction when both mechanical and natural ventilation is present, the absolute velocity values were used to calculate the airflow rates using the VPM. The assumption was that mechanical ventilation prevailed over the natural for the higher fan rotation rates (greater than 15 % of the maximum fan rotation) and that all airstreams in the cavity were directed upward.

When the façade was tested with no mechanical ventilation, the naturally induced airflow was not strong enough to overcome the pressure drop created by the ventilation system attached to the upper DSF opening. As a result, the ultrasonic flowmeter did not register any significant airflow rate in conditions where the
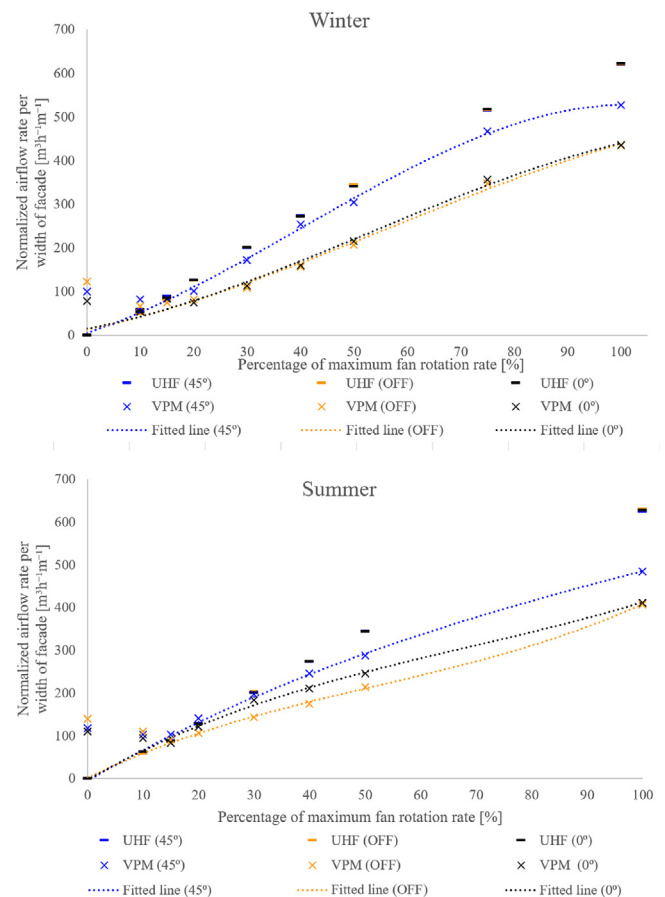

Fig. 9. The normalized airflow rates per width of the façade measured by the UFM and the VPM method. The figure shows the airflow rate profile obtained by fitting the measurements obtained by the UFM and the VPM method.

mechanical ventilation was off. However, the sensors measured the velocities even higher than in certain situations with mechanical ventilation, but the airflow was most likely circulatory in such cases. The gradual increase in fan rotation first caused a decrease in the velocity of the streams initially directed downwards up to the point of changing their direction. Further increase in rotation rate led to steady growth in airspeed. The moment when all currents in the cavity became directed upwards, i.e., when mechanical ventilation prevailed over other circulation paths likely induced by natural phenomena, can be recognized on the graph as the minima in the airflow rates obtained by the VPM method.

The airflow rate profile corresponding to 45° opened venetian blinds shows a certain offset compared to the other two profiles determined by VPM. Having higher airflow rates at a 45° blind angle than in the case without venetians could be expected, as the natural ventilation increases with the closure of the blinds [31]. Therefore, it can be inferred that there was a superposition of natural and mechanical ventilation, which resulted in higher total ventilation rates for the case when the blinds are half-open than in the case without venetian blinds. However, having higher airflow rates than in the case of closed blinds was not expected. That may have originated from the combined effect arising from the punctual measurements of VPM and the nature of the flow. The difference between profiles was evident for the higher airflow rates, where the flow was almost certainly turbulent. Most likely, the drag of partially inclined slats made the flow more turbulent and the velocity profile flatter, resulting in the higher velocity measurements in points close to the channel's borders.

The climate simulator facility also showed a series of limitations, which resulted in certain deviations from the desired conditions for the experimental runs. For example, due to the proximity between the test element and the solar simulator and the inability of the air conditioning system to cool the air in the outer chamber uniformly, the setpoint temperature in the outdoor chamber and air temperature measured near the tested element differed by 2 – 3 ℃. The air temperature in the indoor section was maintained with a stable value at the desired level.

Furthermore, inhomogeneities in solar irradiance registered on the outer surface of the DSF were observed. The lamps' power was adjusted to irradiate the central part of the DSF with 300 Wm^{-2} (winter/mid-season) and 500 Wm^{-2} (summer). The intensity of the radiated energy was stable over time in each of the two sets (winter/mid-season and summer) of experimental runs, with small fluctuations between experimental runs in which different DSF configurations were changed (venetian setup and mechanical ventilation rate). Readings from the thermopile pyranometer in the center point were 500 and 304 Wm^{-2}, while the 5-point averages detected by the photovoltaic pyranometers were 446 and 276 Wm^{-2}, which indicates the inhomogeneity of the solar irradiance on the outer surface of the DSF. The inhomogeneous distribution of the solar irradiance on the DSF's outer surface was observed with a somewhat more pronounced inequality in the replicated conditions corresponding to the winter period (Fig. 10, right). Irregularities are likely to originate from the different hours of usage of light sources, which causes the lamps to change the power emitted with time and by a lower accuracy (of some lamps) in returning the desired radiative flux when a particularly low partial load is adopted. It is possible to see this effect by comparing homogeneity in the case of summer conditions and winter conditions.

Finally, it is also worth noting that the climate simulator also has limitations when it comes to the ability to replicate conditions for radiative long-wave heat exchange between the façade and the surroundings. This limitation might be more relevant when it comes to the radiative heat exchange between the façade and outdoor environment, as it is not possible to replicate the conditions of the sky dome, while the conditions on the side representing the
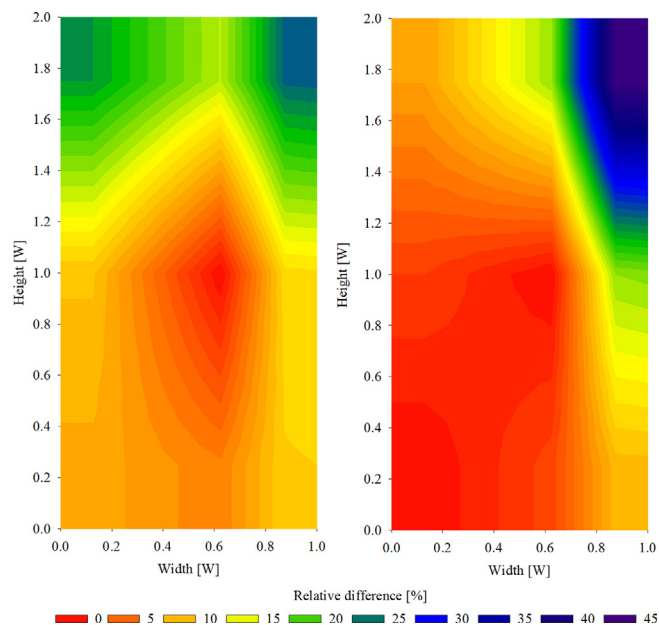

Fig. 10. Distribution of the relative deviation of the solar irradiance measured on the DSF surface in relation to the values measured in the central part for the summer (left) and winter period (right). The dimensions are scaled according to the width of the double glass façade (W).

indoor environment are likely closer to real situations and might therefore not be critical. In general, it is reasonable to expect that the long-wave radiative heat exchange towards the outdoor might have been reduced compared to a real implementation due to higher surface temperatures in the outer chamber of the climate simulator compared to the apparent sky dome temperature.

When it comes to the construction features of the tested DSF mock-up, the chosen glazing configuration of the two skins (two double glazed units) aimed to thermally decouple the cavity from indoor and outdoor environments, allowing us to maximize the collection of solar heat and its transfer to airflow. However, some other glazing configurations could have been chosen, maybe more similar to conventional ones seen in specific types of DSF (e.g., a single glass pane for the outer skin), and therefore a reflection on how this variation might affect the results is probably useful. Let us suppose that the outer skin is realized with a single clear glass (in place of the insulated unit adopted in our experiment). We assume that this leads to an increase in the amount of radiation absorbed by the layers beyond the external skin (as the single glass pane has a lower solar absorptance), especially the shading device and the internal skin, which would lead to greater temperature differences, thus intensifying natural convection and heat transfer in the cavity. Therefore, it is reasonable to expect that the influence of the ventilation rate would increase at the expense of the venetian blinds, as well as that this effect would be more pronounced in mid-season/winter. Perhaps, the influence of venetian blinds may only increase in the case of the indoor glazing temperature, as it is to be expected that the intensification of the airflow occurs primarily in the outer half-cavity and less in the inner half-cavity. However, we believe that the dependence of indicators on these two parameters would not change significantly to alter the overall impression, meaning that in winter, the ventilation rate would continue to be dominant in the control of thermal performance, while in summer, the leading role would still be retained by the venetian blinds.

The research focused on the fresh air requirements of standard office spaces, and therefore we assumed a room depth behind the façade of about 5 m. Yet, a similar assessment could be made for

much deeper spaces that could range up to 25 m in depth [41] – although such an extreme case would probably see different strategies to ensure adequate ventilation and air mixing in the room space, and the role of a transparent façade to determine the indoor environmental quality of the space behind the façade would probably be reduced. In such cases, no more than 3 to 4 persons could fit into a volume near enough the façade to use this space for office work (single or landscape) while preserving a suitable indoor environmental quality. That means that only three to four times higher ventilation rate would be required compared to the selected reference office. This value can easily be achieved with a mechanical ventilation system (1.6 ACH–7 ACH). The experiment results showed that low ventilation rates that sufficiently preheat the air also provide enough fresh air for much deeper spaces (e.g., up to 20 m), considering all building categories. For example, for space with indoor environmental quality in Category I, it would be necessary to provide at least 4.8 ACH, which is still satisfactory in terms of air preheating (Fig. 5a).

Finally, some reflections might also be necessary to link and expand the results of this investigation in relation to the daylighting and visual comfort domain. The impact of DSFs on daylight conditions and challenges and possibilities when it comes to visual comfort has been addressed in a number of previous studies. [42]. Though this is definitely an important domain when it comes to the assessment of the performance of transparent envelope systems, the type of experimental facility used in this study did not allow us to assess the daylight quality provided by the double-skin façade, and to link this behavior to other performance metrics in other domains. The reason for this is that daylighting exploitation, and especially visual comfort, highly depends on the interaction between the façade system and the indoor space, and on the geometrical relationships between the sun, the façade, and the users. In the climate simulators, the solar array is designed to ensure a certain value for (solar) irradiance on the vertical plane parallel to the façade sample, but any geometrical aspects of solar radiation are not replicable. Furthermore, the luminous reflectivity

of the boundary surfaces of the inner chamber, as well as its dimensions, are most likely not representative of typical office space (since they are realized with metal shits). Therefore, any evaluation of illuminance and daylight glare distribution in the inner chamber would be unfounded and hardly applicable to actual conditions. The only proxy for daylighting performance that can be given is to report the measured illuminance on the vertical plane parallel to the façade, and this can give an indication of the potential of the DSF when it comes to enabling daylighting in various combinations of exterior conditions and venetian blind configurations (Fig. 11). Illuminance values are obtained by converting solar irradiance measurements using luminous efficiency of 105 lmW^{-1}, representing the clear sky and average conditions [43]. In the colder part of the year, arrangements without or with semi-open venetian blinds are most optimal when it comes to net heat transfer, while at the same time, they provide plenty of daylight needed for good visual comfort conditions in the interior (Fig. 11). Certainly, for the considered period, it is very unfavorable to have lowered shading, both from thermal and daylighting performance. In contrast, lowered shading is desirable from the aspect of thermal performance of DSFs in tested summer conditions but will most likely not provide enough daylight for the interior. Therefore, the optimal angle likely lies between fully- and semi-enclosed blinds, providing enough light while achieving a sufficiently low net heat transfer between the interior and exterior. As anticipated, more detailed discussions about, for example, glare discomfort risk, cannot be done on the basis of our experimental measurements alone because of the above-mentioned limitation of the testbed employed in this study. However, studies available in literature (as summarised in Table 5 in [44]) showed that an illuminance value on the vertical plane parallel to the façade in the range 3000 to 4000 lx can be assumed, considering the limitations that such a rule-of-thumb may have, as the upper threshold for vertical illuminance values where perception of glare discomfort may begin to appear. With reference to the conditions of the tests carried out in this study, half-opened blinds (blinds tilted so that the
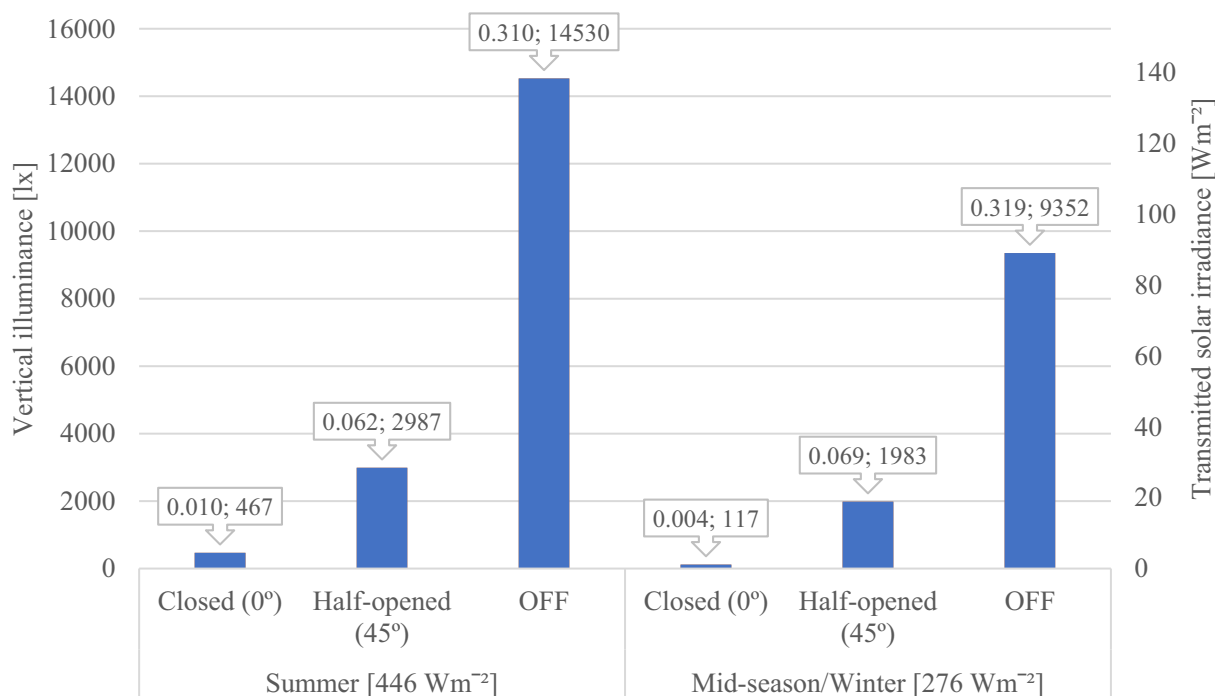

Fig. 11. Illuminance values on the vertical plane parallel to the façade for different combinations of venetian blind configurations and radiated intensities of the solar simulator, calculated from measured values of transmitted irradiance (which can be read on the secondary axis). Values in the squared brackets in the x-axis title give the average values of solar irradiance measured in front of the glazing for two representative cases of boundary conditions. Values in the tags above the columns refer to measured direct solar transmittance (left) and vertical illuminance (right).

angle between the slat and the incoming irradiance vector is 45°) may thus be sufficient to ensure a low risk of glare discomfort.

6. Conclusions

This research has shown that the control of the performance of a one-story DSF may change with the seasons and that airflow rates and venetian blinds can play different roles depending on the boundary conditions and target performance. In the tested winter/mid-season conditions, the thermal behavior of the DSF was regulated to a much greater extent by mechanical ventilation than by venetian blinds. Relatively low ventilation rates were enough to enable positive net heat transfer, while any further rate increase would significantly deteriorate preheating efficiency and net heat transfer. A combination of semi-opened blinds and low ventilation rates was optimal for reduced net heat transfer (energy efficiency) and fresh air delivery (indoor air quality), but also, if one wants to increase the available amount of daylight, which is one of the key advantages of a highly transparent envelope. In the tested summer conditions, the thermal behavior of the DSF was almost entirely regulated by the venetian blinds, while in controlling fluid-dynamics behavior, mechanical ventilation had a primary role, but with the non-negligible influence of venetian blinds. The impact of forced flow on net heat transfer in the tested summer conditions was surprisingly small, indicating that the use of mechanical ventilation in the cavity did not considerably reduce the heat gain through the DSF under steady-state conditions. However, the influence of mechanical ventilation was significant in relieving the excess heat from the cavity, which indicates that the ventilation's impact on the net heat transfer could play a (slightly) more relevant role in transient conditions when the effect of a DSF's thermal inertia is more pronounced.

Though the experimental runs were limited to certain combinations of boundary conditions, we are confident that the chosen boundary conditions were representative enough of "typical" situations, and that therefore the type of functional dependence of the performance output on the different control variables is representative of a larger set of boundary conditions than those employed in the experiments. The research showed the potential of a mechanically ventilated DSF as a dynamic envelope element to act as a device for solar energy exploitation by manipulating the heat collected in the cavity through controllable features. One of the important findings of this paper is that high ventilation rates are not necessary to exploit accumulated heat in the DSF channel efficiently and that relatively low to medium rates can achieve this effect (up to 100 $m^3m^{-1}h^{-1}$). The results of this study can be helpful for researchers working to optimize the size of the HVAC unit, fresh air delivery, air preheating, and utilization of heat collected in the cavity for different purposes.

The experimental data collected during the research activity presented in this paper were made freely available to the scientific community for future independent studies. For instance, the interaction of mechanical ventilation and shading position with construction features that we could not manipulate in experiments (such as the optical properties of glazing or shading devices) could be further examined in numerical studies, or different boundary conditions that were not possible to recreate in a laboratory environment could be adopted to expand the performance analysis.

The experimental data can be found at and referenced using the following weblink: https:// 10.5281/zenodo.6482697/ [11] .

Data availability

Experimental data are available in an online repository as specified in the text of the article.

Declaration of Competing Interest

The authors declare that they have no known competing financial interests or personal relationships that could have appeared to influence the work reported in this paper.

Acknowledgments

References

[1] X. Loncour, A. Deneyer, M. Blasco, G. Flamant, P. Wouters, "Ventilated double facades. Classification & illustration of façade concepts," 2005.

[2] European Committee On Normalization, "NS-EN 12792:2003 Ventilation for buildings - Symbols, terminology and graphical symbols," 2003.

[3] D. Saelens, J. Carmeliet, H. Hens, "Energy performance assessment of multiple-skin facades," Catholic University of Leuven, 2003. https://doi.org/10.1080/10789669.2003.10391063.

[4] X.-l. Xu, Z. Yang, Natural ventilation in the double skin facade with venetian blind, Energy Build. 40 (8) (2008) 1498–1504.

[5] A. Dama, D. Angeli, O.K. Larsen, Naturally ventilated double-skin façade in modeling and experiments, Energy Build. 144 (2017) 17–29, https://doi.org/10.1016/j.enbuild.2017.03.038.

[6] H. Poirazis, *Double skin façades for office buildings*. Lund University, Lund Institute of Technology, 2004.

[7] D. Saelens, Energy Performance Assessment of Single Storey Multiple-Skin Facades, Catholic University of Leuven, 2002.

[8] F. Goia, M. Perino, V. Serra, F. Zanghirella, Towards an active, responsive, and solar building envelope, J. Green Build. 5 (4) (2010) 121–136, https://doi.org/10.3992/jgb.5.4.121.

[9] A. Jankovic, F. Goia, Impact of double skin facade constructional features on heat transfer and fluid dynamic behaviour, Build. Environ. 196 (2021), https://doi.org/10.1016/j.buildenv.2021.107796 107796.

[10] V. Gavan, M. Woloszyn, F. Kuznik, J.-J. Roux, Experimental study of a mechanically ventilated double-skin façade with venetian sun-shading device: a full-scale investigation in controlled environment, Sol. Energy 84 (2) (2010) 183–195. https://doi.org/10.1016/j.solener.2009.10.017.

[11] A. Jankovic and F. Goia, "An experimental data set for analysis of the thermophysical behavior of a single-story mechanically ventilated double-skin façade (DSF) in fixed boundary conditions corresponding to winter/mid-season and summer cases," *2022*. 10.5281/zenodo.6482697.

[12] S. Preet, M.K. Sharma, J. Mathur, A. Chowdhury, S. Mathur, Performance evaluation of photovoltaic double-skin facade with forced ventilation in the composite climate, J. Build. Eng. 32 (2020). https://doi.org/10.1016/j.jobe.2020.101733 101733.

[13] H. Manz, A. Schaelin, H. Simmler, Airflow patterns and thermal behavior of mechanically ventilated glass double facades, Build. Environ. 39 (9) (2004) 1023–1033, https://doi.org/10.1016/j.buildenv.2004.01.003.

[14] S.P. Corgnati, M. Perino, V. Serra, Experimental assessment of the performance of an active transparent façade during actual operating conditions, Sol. Energy 81 (8) (2007) 993–1013. https://doi.org/10.1016/j.solener.2006.12.004.

[15] A. Hazem, M. Ameghchouche, C. Bougriou, A numerical analysis of the air ventilation management and assessment of the behavior of double skin facades, Energy Build. 102 (2015) 225–236, https://doi.org/10.1016/j.enbuild.2015.05.057.

[16] J. Parra, A. Guardo, E. Egusquiza, P. Alavedra, Thermal performance of ventilated double skin façades with venetian blinds, Energies 8 (6) (2015) 4882–4898, https://doi.org/10.3390/en8064882.

[17] T. Inan, T. Basaran, A. Erek, Experimental and numerical investigation of forced convection in a double skin façade, *Energies* 10 (9) (2017), https://doi.org/10.3390/en10091364.

[18] N. Safer, Modélisation des façades de type double-peau équipées de protections solaires : Approches multi-échelles, L'Institut National des Sciences Appliquées de Lyon, 2006.

[19] A. Guardo, M. Coussirat, E. Egusquiza, P. Alavedra, R. Castilla, A CFD approach to evaluate the influence of construction and operation parameters on the performance of Active Transparent Façades in Mediterranean climates, Energy Build. 41 (5) (2009) 534–542, https://doi.org/10.1016/j.enbuild.2008.11.019.

[20] N. Safer, M. Woloszyn, J.J. Roux, Three-dimensional simulation with a CFD tool of the airflow phenomena in single floor double-skin facade equipped with a venetian blind, Sol. Energy 79 (2) (2005) 193–203. https://doi.org/10.1016/j.solener.2004.09.016.

[21] T.E. Jiru, Y.X. Taob, F. Haghighat, Airflow and heat transfer in double skin facades, Energy Build. 43 (10) (2011) 2760–2766, https://doi.org/10.1016/j.enbuild.2011.06.038.

[22] R. Fuliotto, F. Cambuli, N. Mandas, N. Bacchin, G. Manara, Q. Chen, Experimental and numerical analysis of heat transfer and airflow on an interactive building facade, Energy Build. 42 (1) (2010) 23–28. https://doi.org/10.1016/j.enbuild.2009.07.006.

[23] E. Oesterle, R.-D. Lieb, M. Lutz, W. Heusler, Double-skin Facades: Integrated Planning, Prestel, München, 2001.

[24] S. Preet, J. Mathur, S. Mathur, Influence of geometric design parameters of double skin façade on its thermal and fluid dynamics behavior: a comprehensive review, Sol. Energy 236 (2022) 249–279. https://doi.org/10.1016/j.solener.2022.02.055.

[25] O. Aleksandrowicz, A. Yezioro, Mechanically ventilated double-skin facade in a hot and humid climate: summer monitoring in an office tower in Tel Aviv, Archit. Sci. Rev. 61 (3) (2018) 171–188, https://doi.org/10.1080/00038628.2018.1450726.

[26] M. Bhamjee, A. Nurick, D.M. Madyira, An experimentally validated mathematical and CFD model of a supply air window: forced and natural flow, Energy Build. 57 (2013) 289–301, https://doi.org/10.1016/j.enbuild.2012.10.043.

[27] J.S. Carlos, H. Corvacho, P.D. Silva, J.P. Castro-Gomes, Modelling and simulation of a ventilated double window, Appl. Therm. Eng. 31 (1) (2011) 93–102. https://doi.org/10.1016/j.applthermaleng.2010.08.021.

[28] I. Pérez-Grande, J. Meseguer, G. Alonso, Influence of glass properties on the performance of double-glazed facades, Appl. Therm. Eng. 25 (17–18) (2005) 3163–3175, https://doi.org/10.1016/j.applthermaleng.2005.04.004.

[29] D. Faggembauu, "Heat transfer and fluid-dynamics in double and single skin facades," Universitat Politècnica de Catalunya, 2006.

[30] A. Jankovic, M.S. Siddiqui, F. Goia, Laboratory testbed and methods for flexible characterization of thermal and fluid dynamic behaviour of double skin facades, Build. Environ. 210 (2022). https://doi.org/10.1016/j.buildenv.2021.108700 108700.

[31] A. Jankovic, F. Goia, Characterization in a controlled environment of a naturally ventilated double-skin façade through the design of experiments (DOE) methodology, Energy Build (2022) 112024, https://doi.org/10.1016/j.enbuild.2022.112024.

[32] International Organization for Standardization, "ISO 9060:2018(en) Solar energy — Specification and classification of instruments for measuring hemispherical solar and direct solar radiation," 2018.

[33] A. Jankovic, G. Chaudhary, F. Goia, Designing the design of experiments (DOE) – An investigation on the influence of different factorial designs on the characterization of complex systems, Energy Build. 250 (2021). https://doi.org/10.1016/j.enbuild.2021.111298 111298.

[34] International Organization for Standardization, "ISO 15099: 2003 Thermal performance of windows, doors and shading devices," 2003.

[35] M.L. Chereches et al., Experimental study on airflow and temperature predicting in a double skin Façade in hot and cold seasons in Romania, Appl. Sci. 11 (24) (2021), https://doi.org/10.3390/app112412139.

[36] F. Di Maio, A.H.C. van Paassen, Modelling the air infiltrations in the second skin facade, in: in Proceedings of the 4th international conference on indoor air quality, ventilation and energy conservation in buildings, 2001, pp. 873–880.

[37] International Organization for Standardization, "EN 16798-1:2019 Energy performance of buildings - Ventilation for buildings - Part 1: Indoor environmental input parameters for design and assessment of energy performance of buildings addressing indoor air quality, thermal environment, lighting and acous," 2019.

[38] International Organization for Standardization, "SN-CEN/TR 16798-2:2019 Energy performance of buildings - Ventilation for buildings - Part 2: Interpretation of the requirements in EN 16798-1 - Indoor environmental input parameters for design and assessment of energy performance of buildings addressing i," 2019.

[39] C. Popa, D. Ospir, S. Fohanno, C. Chereches, Numerical simulation of dynamical aspects of natural convection flow in a double-skin façade, Energy Build. 50 (2012) 229–233, https://doi.org/10.1016/j.enbuild.2012.03.042.

[40] A. Jankovic, G. Gennaro, G. Chaudhary, F. Goia, F. Favoino, Tracer gas techniques for airflow characterization in double skin facades, Build. Environ. 212 (2022). https://doi.org/10.1016/j.buildenv.2022.108803 108803.

[41] R. Garay-Martinez, B. Arregi, J. Kurnitski, T. Kalamees, Curtain wall with solar preheating of ventilation air. full scale experimental assessment, E3S Web Conf. 172 (2020) 09007.

[42] M.A. Shameri, M.A. Alghoul, K. Sopian, M.F.M. Zain, O. Elayeb, Perspectives of double skin façade systems in buildings and energy saving, Renew. Sustain. Energy Rev. 15 (3) (2011) 1468–1475, https://doi.org/10.1016/j.rser.2010.10.016.

[43] P.J. Littlefair, The luminous efficacy of daylight: a review, Light. Res. Technol. 17 (4) (1985) 162–182, https://doi.org/10.1177/14771535850170040401.

[44] L. Giovannini, F. Favoino, V.R.M. Lo Verso, V. Serra, A. Pellegrino, GLANCE (GLare ANnual Classes Evaluation): an approach for a simplified spatial glare evaluation, Build. Environ. 186 (2020), https://doi.org/10.1016/j.buildenv.2020.107375 107375.

[45] F. Goia, V. Serra, Analysis of a non-calorimetric method for assessment of in-situ thermal transmittance and solar factor of glazed systems, Sol. Energy 166 (2018) 458–471, https://doi.org/10.1016/j.solener.2018.03.058.